

# Surface scaling behavior of isotropic Heisenberg systems: Critical exponents, structure factor, and profiles

Michael Krech

*Fachbereich Physik, Bergische Universität - GH Wuppertal, 42097 Wuppertal  
Federal Republic of Germany*

The surface scaling behavior of classical isotropic Heisenberg magnets is investigated by Monte - Carlo methods in  $d = 3$  dimensions for various values of the surface - to - bulk coupling ratio  $J_1/J$ . For  $J_1/J \leq 1.0$  critical behavior according to the ordinary surface universality class is found. New estimates for magnetic surface exponents are presented and compared to older estimates and their theoretical counterparts. For  $J_1/J \geq 2.0$  scaling is still valid with effective exponents which depend on  $J_1/J$ . The surface structure factor  $S_1(p, L)$  is investigated at bulk criticality as function of the momentum transfer  $p$  parallel to the surface and the system size  $L$ . For  $J_1/J \leq 1.0$  and  $J_1/J \geq 2.0$  the full  $p$  dependence of  $S_1(p, L)$  can be captured by generalized shape functions to a remarkable accuracy. Profiles of the magnetization and the energy density also confirm scaling, where for  $J_1/J \leq 1.0$  the ordinary surface universality class is recovered and for  $J_1/J \geq 2.0$  scaling with  $J_1/J$  dependent exponents is found. For  $J_1/J = 1.5$  the system displays a striking crossover behavior from spurious long - range surface order to the ordinary surface universality class. For  $J_1/J \geq 2.0$  the effective scaling laws must be interpreted as nonasymptotic and the value  $J_1/J = 1.5$  marks a crossover regime, in which the crossover from the nonasymptotic to the asymptotic (ordinary) surface scaling behavior can be resolved within numerically attainable system sizes.

PACS numbers: 75.10.Hk, 68.35.Rh, 64.60.Fr, 05.70.Jk

## I. INTRODUCTION

Classical spin systems with  $O(N)$  symmetry display long - range magnetic order at low temperatures, if the spatial dimensionality is sufficiently high or the interaction range is sufficiently large. Long - range order sets in spontaneously below a certain critical temperature  $T = T_c$  at zero magnetic field  $\mathbf{H} = \mathbf{0}$ , where the field  $\mathbf{H}$  has  $N$  components. In the vicinity of the critical point  $(T, \mathbf{H}) = (T_c, \mathbf{0})$  these systems are characterized by an  $N$  component order parameter given by the magnetization. Both from the theoretical and the experimental point of view these systems provide important realizations of the well known  $O(N)$  universality class for critical behavior. In particular, the cases  $N = 1$ ,  $N = 2$ , and  $N = 3$  are most relevant for experiments, because they correspond to the Ising universality class (magnets with uniaxial anisotropies, simple and binary fluids), the XY universality class (magnets with planar anisotropies,  $^4\text{He}$  near the normal - superfluid transition), and the Heisenberg universality class (isotropic magnets, e.g. Ni, EuO, EuS), respectively. Real samples of any material always have surfaces which display a distinct critical behavior in the vicinity of the critical point of the bulk material. In turn, the penetration depth of surface effects is set by the bulk correlation length  $\xi = \xi_{\pm}^0 |\tau|^{-\nu}$  which *diverges* at the critical point  $\tau = (T - T_c)/T_c \rightarrow 0$ , where  $\mathbf{H} = \mathbf{0}$  is assumed. The exponent  $\nu$  is the *universal* correlation length exponent and  $\xi_{\pm}^0$  denotes the nonuniversal correlation length amplitudes above (+) and below (-)  $T_c$  ( $N = 1$  only). It is now well established that surface critical behavior obeys the principle of universality, i.e., critical exponents and scaling functions which character-

ize surface critical behavior do not depend on microscopic details of the material<sup>1-3</sup>. General field - theoretic considerations based on the  $\phi^4$  Ginzburg - Landau model for semiinfinite systems<sup>2,3</sup> show that for  $O(N)$  symmetric systems there are three surface universality classes which are denoted as *ordinary* ( $O$ ), *surface - bulk* or *special* ( $SB$ ), and *extraordinary* ( $E$ ). These three universality classes can be briefly characterized by the absence or presence of surface order at the critical point of the bulk material. In particular,  $O$  stands for a *disordered* surface and  $E$  symbolizes an ordered surface, whereas  $SB$  indicates that surface and bulk are critical simultaneously. The physical nature of the  $SB$  surface universality class is that of a *multicritical point*<sup>2</sup>. Surface order can arise spontaneously ( $E$ ) or can be imposed from outside by a surface field  $\mathbf{H}_1$ . The latter case is quite common in fluid systems with confining walls (Ising universality class,  $N = 1$ )<sup>4</sup>, where the bulk transition is then denoted as *normal transition*. It has been shown by rigorous arguments, that apart from corrections to scaling the normal and the extraordinary transition are equivalent<sup>5</sup>. This is also quite important for the theory, because the normal transition gives access to the extraordinary surface universality class even when the surface does not order spontaneously, i.e., the  $SB$  multicritical point does not exist.

Within the framework of  $O(N)$  symmetric spin models on lattices we will only consider the case of short - range interactions which is characterized by a nearest - neighbor coupling constant  $J$  in the bulk and by another nearest - neighbor coupling constant  $J_1$  in the surface. In this case the absence or presence of the  $SB$  transition crucially depends on the spatial dimension  $d$  and the value

of  $N$ . In  $d = 2$  dimensions the  $SB$  transition does not exist, because the "surfaces" in this case are only one - dimensional. Note that for  $N \geq 2$  a  $O(N)$  spin system does not show long - range order in  $d = 2$ <sup>6</sup>. In  $d = 3$  the value of  $N$  becomes crucial. For  $N = 1$  the  $SB$  transition exists, because the surface, i.e., the Ising model in  $d = 2$ , exhibits long - range order below a finite critical temperature. In the phase diagram of a semi - infinite Ising ferromagnet the  $SB$  multicritical point is located at  $T = T_c$ ,  $\mathbf{H} = \mathbf{H}_1 = 0$  ( $N = 1$  here), and the critical value  $J_1^c/J$  of the surface - to - bulk coupling ratio  $J_1/J$ . Note that besides the lines of the  $O$  and  $E$  transitions a line of *surface transitions* terminates in the  $SB$  multicritical point<sup>1,2</sup>. For the Ising ferromagnet one finds  $J_1^c/J = 3/2$  on a simple cubic lattice to a remarkably high accuracy<sup>7</sup>. For  $N = 2$  the surface of the spin system is a two - dimensional XY model which does no longer show long - range order<sup>6</sup>. Instead, a line of Kosterlitz - Thouless surface transitions occurs in the  $(T, J_1/J)$  plane of the phase diagram<sup>8</sup> which terminates in a  $SB$  multicritical point at  $T = T_c$  and  $J_1/J = J_1^c/J \simeq 1.5$  for a XY ferromagnet on a simple cubic lattice. For  $N = 3$  the  $SB$  transition does not exist, because the two - dimensional Heisenberg model has no phase transition<sup>6</sup>. In the absence of symmetry breaking surface interactions the isotropic Heisenberg ferromagnet in  $d = 3$  should therefore always display *ordinary* surface critical behavior, regardless of the value of  $J_1/J$ . In  $d \geq 4$  dimensions, i.e., within mean - field theory, the  $SB$  transition exists for any value of  $N$ .

The dimensional crossover behavior of the  $SB$  multicritical point outlined above greatly complicates the field - theoretic description of the  $SB$  transition for general  $N$ , apart from additional Goldstone problems below  $T_c$  for  $N > 1$ <sup>9</sup> which can be accounted for in finite systems with periodic boundary conditions<sup>10</sup>. Therefore, most of the field - theoretic work is devoted to the Ising universality class and to the ordinary transition for general  $N \geq 1$ <sup>2,11,12</sup>. In the following we will focus on the ordinary transition in isotropic Heisenberg magnets and we therefore only summarize some aspects of the ordinary surface universality class for later reference. For a recent general survey of surface critical behavior the reader is referred to Ref.<sup>3</sup>.

Apart from the standard bulk critical exponents additional surface critical exponents must be introduced in order to describe critical behavior at the ordinary transition. Let  $m_1$  denote the modulus of the surface magnetization per spin  $\mathbf{M}_1/\text{Area}$  and let  $H$  and  $H_1$  denote the moduli of the bulk and surface field  $\mathbf{H}$  and  $\mathbf{H}_1$ , respectively. Then the critical behavior of  $m_1$  and of the susceptibilities  $\chi_1$  and  $\chi_{11}$  is given by<sup>1,2,11</sup>

$$\begin{aligned} m_1 &\sim (-\tau)^{\beta_1} \\ \chi_1 &= \frac{\partial m_1}{\partial H} \sim |\tau|^{-\gamma_1} \\ \chi_{11} &= \frac{\partial m_1}{\partial H_1} \sim |\tau|^{-\gamma_{11}} \end{aligned} \quad (1.1)$$

for  $H = H_1 = 0$  and sufficiently small  $\tau$ . The susceptibilities  $\chi_1$  and  $\chi_{11}$  are known as the layer susceptibility and the surface or local susceptibility. In terms of the coordinates  $\mathbf{x}_{||}$  parallel to the surface and  $z$  perpendicular to the surface the correlation decay exponents  $\eta_{||}$  and  $\eta_{\perp}$  are defined by<sup>1,2</sup>

$$\begin{aligned} G(|\mathbf{x}_{||} - \mathbf{x}'_{||}|, z, z) &\sim |\mathbf{x}_{||} - \mathbf{x}'_{||}|^{-(d-2+\eta_{||})} \\ G(0, z, z') &\sim |z - z'|^{-(d-2+\eta_{\perp})} \end{aligned} \quad (1.2)$$

in the limit of large distances, where  $T = T_c$  and  $H = H_1 = 0$  is assumed. The surface exponents defined in Eqs.(1.1) and (1.2) are not independent. By virtue of the scaling relations<sup>1,2</sup>

$$\begin{aligned} \beta_1 &= \nu(d - 2 + \eta_{||})/2 \\ \gamma_1 &= \nu(2 - \eta_{\perp}) \\ \gamma_{11} &= \nu(1 - \eta_{||}) \\ \eta_{\perp} &= (\eta + \eta_{||})/2 \end{aligned} \quad (1.3)$$

only one of the surface exponents defined above, say,  $\eta_{||}$  is independent for given  $\nu$  and  $\eta$ , where  $\eta$  is the decay exponent of the bulk correlation function according to  $G(|\mathbf{x}^{(1)} - \mathbf{x}^{(2)}|) \sim |\mathbf{x}^{(1)} - \mathbf{x}^{(2)}|^{-(d-2+\eta)}$  at  $T = T_c$ . The remaining magnetic exponents  $\delta_1$  and  $\delta_{11}$  defined by

$$\begin{aligned} m_1(T_c, H, H_1 = 0) &\sim H^{1/\delta_1} \\ m_1(T_c, H = 0, H_1) &\sim H_1^{1/\delta_{11}} \end{aligned} \quad (1.4)$$

are related to the bulk exponents  $\nu$  and  $\eta$  and the surface exponent  $\eta_{||}$  according to  $\delta_1 = \nu(d + 2 - \eta)/(2\beta_1)$  and  $\delta_{11} = \nu(d - \eta_{||})/(2\beta_1)$ , respectively<sup>1,2</sup>. In analogy with Eq.(1.1) the layer specific heat  $C_1$  and the surface or local specific heat  $C_{11}$  display the critical singularities<sup>1,2</sup>

$$\begin{aligned} C_1 &= \frac{\partial e_1}{\partial t} \sim |\tau|^{-\alpha_1} \\ C_{11} &= \frac{\partial e_1}{\partial c} \sim |\tau|^{-\alpha_{11}}, \end{aligned} \quad (1.5)$$

where  $e_1$  is the surface energy density per spin and  $c = (J_1^c - J_1)/J$  is the surface enhancement. Within the framework of the field - theoretic renormalization group it has been shown by an explicit calculation of the energy density profile<sup>13</sup> and from the short - distance expansion of the energy density operator near the surface<sup>14,15</sup> that  $\alpha_1 = \alpha - 1$  and  $\alpha_{11} = \alpha - 2 - \nu$  at the ordinary transition. The critical singularities of all bulk and surface quantities can therefore be expressed by the bulk exponents  $\nu$  and  $\eta$  and the surface exponent  $\eta_{||}$ , i.e., there is only a single independent surface exponent at the ordinary transition<sup>2</sup>. Within the field - theoretic renormalization group in  $d = 4 - \varepsilon$  all surface exponents are known to two - loop order for general  $N$ <sup>2,11</sup>. The extrapolation of the  $\varepsilon$  - expansion to  $d = 3$  ( $\varepsilon = 1$ ) already yields reasonable estimates for the surface exponents, however, their numerical accuracy remains unknown due to the lack of higher order results which are needed to apply resummation techniques. Therefore, alternative analytic approaches have

been pursued in order to obtain improved estimates. In particular for the Heisenberg model  $\beta_1 = 0.81 \pm 0.04$  has been obtained<sup>16</sup> which agrees with the extrapolated value for  $\beta_1$ <sup>2</sup>. The result of a perturbative calculation for the nonlinear sigma model in  $d = 2 + \varepsilon$  has been combined with the results in  $d = 4 - \varepsilon$  by means of a Padé approximant<sup>17</sup> resulting in the numerical estimates  $\beta_1 = 0.84 \pm 0.01$  and  $\eta_{||} = 1.39 \pm 0.02$ . A massive field-theoretic approach recently provided the new estimates  $\beta_1 = 0.880, 0.862, 0.889$  from a  $[2/0]$ ,  $[0/2]$ , and  $[1/1]$  Padé approximant in  $d = 3$ , respectively<sup>12</sup>. From an earlier experiment on Ni(100) and Ni(110) surfaces<sup>18</sup> the average estimates  $\beta_1 \simeq 0.81$  and  $\beta_1 \simeq 0.79$  have been obtained, respectively.

For the experimental verification of surface critical behavior<sup>18</sup> the structure factor in surfaces and thin films is of particular interest<sup>19</sup>. From Eq.(1.2) one concludes that for small parallel momentum transfer  $p$  the surface correlation function displays the algebraic  $p^{-1+\eta_{||}}$  singularity, which gives access to the exponent  $\eta_{||}$  in a surface scattering experiment. Consequently, substantial theoretical effort has been spent on the theoretical understanding of correlation functions in surfaces and films<sup>20</sup> and the crossover behavior between them<sup>21</sup>. A thorough survey of the properties of the static structure factor can be found in Ref.<sup>22</sup>. Scattering experiments also give access to the order parameter profile which is governed by universal shape functions. In  $d = 2$  and at  $T = T_c$  the shape functions of the order parameter and the energy density profile for Ising and Potts models can be obtained from conformal invariance considerations<sup>23</sup>. Generalizations to  $O(N)$  symmetric models in  $d = 2$  are also possible<sup>24</sup>. In higher dimensions one has to resort to field - theoretic methods<sup>13,25</sup>, where only the energy density profile is nonzero at the ordinary transition<sup>13,26</sup>. The identification of the surface universality class for a specific system is a rather delicate problem. For example, the presence of weak surface fields leads to a *crossover* from ordinary to extraordinary behavior as the surface is approached from the interior<sup>27</sup>. For multi - component systems, e.g., binary alloys the surface universality classes may even be different for different *orientations* of the surface<sup>28</sup>.

Whereas most of the theoretical results quoted above can be applied to the case  $d = 3$ ,  $N = 3$  under consideration, numerical investigations have primarily focussed on the Ising universality class ( $N = 1$ ) in  $d = 3$ . From a Monte - Carlo simulation of the isotropic Heisenberg ferromagnet on a simple cubic lattice with an open surface on one side and a self - consistently determined surface field on the opposite side<sup>29</sup> an estimate  $\beta_1 = 0.75 \pm 0.10$  has been found for the surface exponent  $\beta_1$  (ordinary transition)<sup>30</sup>. The field dependence of the surface magnetization  $m_1$  at  $T = T_c$  (see Eq.(1.4)) was determined later<sup>31</sup> and the estimate  $\delta_1 = 2.3 \pm 0.1$  was found. Transfer matrix Monte - Carlo calculations for the Heisenberg ferromagnet on small lattices provided the estimate  $\beta_1 = 0.80 \pm 0.03$ <sup>32</sup>. Most of the numerical effort has been spent on the surface critical behavior of the Ising model<sup>33</sup>

and a few detailed studies also exist for the XY model<sup>34</sup>. The most accurate numerical estimates of Ising surface exponents and amplitude ratios at the ordinary and the SB transition can be found in Ref.<sup>7</sup>. We close this brief overview with the remark that the surface exponent  $\beta_1$  for the ordinary transition is not affected by surface bond disorder or the presence of steps on the surface<sup>35</sup>. A theoretical explanation for this behavior can be found from the construction of upper and lower bounds on  $\beta_1$ <sup>36</sup>.

Although a substantial wealth of information is already available for the surface critical behavior of the isotropic ferromagnet with  $O(N = 3)$  symmetry at the surface, the resulting estimates for the surface critical exponents are too disparate to provide a reliable basis for further investigations, e.g. the surface contribution to the dynamic structure factor. Furthermore, a systematic scaling analysis of static surface correlations is still missing, which provides essential information for the numerical analysis of experimental scattering data and Monte - Carlo data of the dynamic structure factor. Moreover, previous investigations were focussed on the *asymptotic* scaling regime of the ordinary surface universality class. In real systems or computer simulations of isotropic Heisenberg magnets, however, the surface properties at hand may be such that asymptotic scaling is only obtained after a crossover regime of a certain width has been traversed. This also means that some sort of nonasymptotic surface behavior must occur before the crossover regime is reached even if the bulk is already critical, i.e., displays asymptotic scaling behavior governed by bulk exponents. It is important for the analysis of numerical data to localize these regimes and to describe their properties.

It is the purpose of this investigation to fill at least some of the aforementioned gaps. In particular new independent estimates for the surface critical exponents of the isotropic Heisenberg ferromagnet at the ordinary transition are provided. With Refs.<sup>22</sup> and<sup>26</sup> as guidelines for the universal form of the shape functions the surface structure factor and the order parameter and energy density profiles are analyzed at  $T = T_c$  for various values of the surface - to - bulk coupling ratio  $J_1/J$ . Particular attention will be paid to the crossover regime, which is best described by the shape crossover of order parameter and energy density profiles. Outside the crossover regime a nonasymptotic scaling regime is investigated and characterized by nonuniversal  $J_1/J$  dependent exponents. This work is mainly focussed on scaling properties and therefore the simulations are restricted to simple cubic lattices with (100) surfaces.

## II. MODEL AND SIMULATION METHOD

The model Hamiltonian describes an isotropic Heisenberg ferro - or antiferromagnet on a simple cubic lattice with two (100) surfaces in a cubic geometry. It is given

by (see also Ref.<sup>7</sup>)

$$\mathcal{H} = -J \sum_{\langle i,j \rangle \in V \setminus A} \mathbf{S}_i \cdot \mathbf{S}_j - J_1 \sum_{\langle i,j \rangle \in A} \mathbf{S}_i \cdot \mathbf{S}_j, \quad (2.1)$$

where  $V$  denotes the set of all lattice sites (volume) and  $A$  denotes the set of surface sites. The coupling constants  $J$  and  $J_1$  are assumed to have the same sign and the spins  $\mathbf{S}_i = (S_i^x, S_i^y, S_i^z)$  with  $|\mathbf{S}_i| = 1$  only interact with nearest neighbors. A nearest neighbor pair  $\langle i, j \rangle$  of spins is part of the interior  $V \setminus A$  of the system, if at least one of the spins is not part of the surface  $A$ . A nearest neighbor pair  $\langle i, j \rangle$  is part of the surface if both spins belong to  $A$ . The surfaces are defined by the lattice planes  $(x, y, z = 1)$  and  $(x, y, z = L)$ , where  $1 \leq x, y \leq L'$ . Along the  $x$  and  $y$  directions periodic boundary conditions are applied. In order to avoid unwelcome finite - size effects the geometry of the lattice is chosen as cubic, i.e.,  $L' = L$ . The cubic shape turns out to be a reasonable compromise between achievable system sizes  $L$  and the sensitivity of the system to the surface - to - bulk coupling ratio  $J_1/J$ .

The Monte - Carlo algorithm is chosen as a hybrid scheme which consists of Metropolis sweeps, Wolff single cluster updates<sup>38</sup>, and overrelaxation sweeps<sup>37</sup>. Typically, one hybrid Monte - Carlo step consists of 10 individual steps each of which can be one of the updates listed above. The Metropolis and the Wolff algorithm work the standard way, where the reduced coordination number of the lattice at the surfaces and the modified surface coupling  $J_1$  must be taken into account. The acceptance probability  $p$  of a proposed spin flip in the Metropolis algorithm is defined by  $p(\Delta E) = 1/[\exp(\Delta E/k_B T) + 1]$ , where  $k_B$  is the Boltzmann constant and  $\Delta E$  is the change in configurational energy of the proposed move. The overrelaxation part of the algorithm performs a microcanonical update of the configuration by sequentially rotating each spin in the lattice such that its energy contribution to the energy of the whole configuration remains constant. The implementation of this update scheme is straightforward, because according to Eq.(2.1) the energy of a spin with respect to its neighborhood has the functional form of a scalar product. The angle of rotation can be chosen randomly for each spin, however, it turns out that in view of minimal autocorrelation times a reflection, i.e., a rotation of all spins by 180 degrees is the most efficient overrelaxation move. One hybrid Monte - Carlo step consists of two Metropolis (M) for single cluster Wolff (C) and four overrelaxation (O) updates. The individual updates are mixed automatically in the program to generate the update sequence M O C O C M O C O C. The random number generator is the shift register generator R1279 defined by the recursion relation  $X_n = X_{n-p} \oplus X_{n-q}$  for  $(p, q) = (1279, 1063)$ . Generators like these are known to cause systematic errors in combination with the Wolff algorithm<sup>39</sup>. However, for lags  $(p, q)$  used here these errors are far smaller than typical statistical errors. They are further reduced by the hybrid nature of the algorithm<sup>40</sup>.

The Monte - Carlo scheme described above is employed for lattice sizes  $L$  between  $L = 12$  and  $L = 72$ . For each choice of parameters we perform at least 20 blocks of  $10^3$  hybrid steps for equilibration followed by  $10^4$  hybrid steps for measurements. Each measurement block yields an estimate for all quantities of interest and from these we obtain our final estimates and estimates of their statistical error following standard procedures. The integrated autocorrelation time of the hybrid algorithm is determined by the autocorrelation function of the energy or, equivalently, the modulus of the magnetization, which yield the slowest modes for the Wolff algorithm. The autocorrelation times do not exceed 10 hybrid Monte - Carlo steps for the largest lattice size ( $T = T_c$ ), so the equilibration and measurement periods quoted above translate to roughly 100 and 1000 autocorrelation times, respectively. In order to obtain the best statistics for all magnetic quantities a measurement is made after every hybrid Monte - Carlo step. All error bars quoted in the following correspond to one standard deviation. The hybrid scheme samples the surfaces of the system reasonably often, so a preferential sampling of surface configurations is not required. The simulations have been performed on DEC alpha and AXP workstations at the Physics department of the BUGH Wuppertal.

### III. SURFACE SCALING EXPONENTS

The simulations presented here have been performed at  $T = T_c$  for several values of the surface - to - bulk coupling ratio  $J_1/J$ . The estimate for  $T_c$  used here is taken from Ref.<sup>37</sup>, where the critical coupling  $K_c$  has been determined as  $K_c \equiv J/(k_B T_c) = 0.693035(37)$ . In view of the limited system size  $L \leq 72$  the relative accuracy of  $10^{-4}$  in  $T_c$  is sufficient in order to perform a standard finite - size scaling analysis in terms of the system size  $L$  up to the usual corrections to scaling. As our main reference for bulk critical exponents we choose the work of Guida and Zinn - Justin<sup>41</sup>, where the bulk critical exponents of the  $O(N)$  universality class have been obtained from high order Borel resummed perturbation theory for the Ginzburg - Landau model.

In order to access surface critical exponents the surface magnetization  $m_1$ , its second moment, and the surface energy density  $e_1$  has been measured. The layer and surface specific heats  $C_1$  and  $C_{11}$  (see Eq.(1.5)) have not been investigated, because  $\alpha_1$  and  $\alpha_{11}$  can be expressed by bulk exponents only. The layer magnetization  $\mathbf{m}(z)$ ,  $1 \leq z \leq L$  and the total magnetization  $\mathbf{m}_{tot}$  are defined by

$$\mathbf{m}(z) \equiv \sum_{x,y=1}^L \mathbf{S}_{xyz}/L^2 \quad (3.1)$$

$$\mathbf{m}_{tot} \equiv \sum_{z=1}^L \mathbf{m}(z)/L,$$

respectively, and  $m_{tot} \equiv |\mathbf{m}_{tot}|$  denotes the modulus of the total magnetization. The magnetization profile  $m(z)$  is then defined as the projection of  $\mathbf{m}(z)$  onto the total magnetization  $\mathbf{m}_{tot}$ , i.e.,

$$m(z) \equiv \mathbf{m}(z) \cdot \mathbf{m}_{tot}/m_{tot} \quad (3.2)$$

and  $m_1 \equiv (m(1) + m(L))/2$  defines the surface magnetization. Note that the surfaces at  $z = 1$  and  $z = L$  are identical (see Eq.(2.1)). In terms of  $m_{tot}$  and  $m_1$  the layer and surface susceptibilities (i.e., their longitudinal components)  $\chi_1$  and  $\chi_{11}$  for a completely finite system are defined as

$$\begin{aligned} \chi_1 &= L^2(\langle m_{tot} m_1 \rangle - \langle m_{tot} \rangle \langle m_1 \rangle)/(k_B T) \\ \chi_{11} &= L^2(\langle m_1^2 \rangle - \langle m_1 \rangle^2)/(k_B T), \end{aligned} \quad (3.3)$$

where  $\langle \dots \rangle$  denotes the thermal average. The energy profile  $e(z)$  is defined accordingly, where apart from the exchange energy between the spins *within* layer  $z$  half the interaction energy to the layers  $z - 1$  and  $z + 1$  also contributes to  $e(z)$ , so  $e_{tot} \equiv \sum_{z=1}^L e(z)/L$  is the total energy density. In the following all energies will be given in units of  $k_B T_c$ , i.e., extra factors  $k_B T$  (see, e.g, Eq.(3.3)) are unity at  $T = T_c$ .

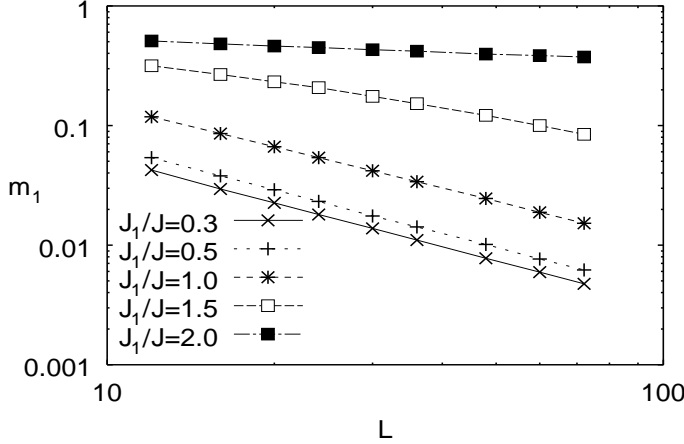


FIG. 1. Surface magnetization  $m_1(L)$  (see Eq.(3.2)) at  $T = T_c$  as function of the system size  $L$  for  $J_1/J = 0.3$  ( $\times$ , solid line),  $0.5$  ( $+$ , short dashed line),  $1.0$  ( $*$ , dashed line),  $1.5$  ( $\square$ , long dashed line), and  $2.0$  ( $\blacksquare$ , dash-dotted line). Statistical errors are much smaller than the symbol sizes and the various lines are just guides to the eye. For  $J_1/J \leq 1$   $m_1$  displays the expected behavior for the ordinary surface universality class. For  $J_1/J = 1.5$  the system undergoes a crossover towards ordinary surface behavior, whereas for  $J_1/J = 2.0$  the behavior of  $m_1$  is inherently nonasymptotic within the available range of system sizes.

The surface magnetization  $m_1$  at  $T = T_c$  as function of the system size  $L$  is shown in Fig.1 for  $J_1/J = 0.3$ ,

$0.5$ ,  $1.0$ ,  $1.5$ , and  $2.0$ . For  $J_1/J \leq 1$  the functional form of  $m_1(L) \equiv \langle m_1 \rangle$  is accurately captured by

$$m_1(L) = B_{m_1} L^{-\beta_1/\nu} (1 + C_{m_1} L^{-\omega}), \quad (3.4)$$

where  $B_{m_1}$  is the magnetization amplitude and  $C_{m_1}$  is the amplitude of the leading correction to scaling. The associated Wegner exponent  $\omega = 0.78$  is taken from Ref.<sup>41</sup>. A least square fit of Eq.(3.4) to the data for  $J_1/J \leq 1$  displayed in Fig.1 yields the estimates  $\beta_1/\nu = 1.185(6)$ ,  $1.175(13)$ , and  $1.171(7)$  for  $J_1/J = 0.3$ ,  $0.5$ , and  $1.0$ , respectively. The error indicated in parenthesis corresponds to one standard deviation. From these estimates one obtains the weighted average  $\beta_1/\nu = 1.179(6)$ , where the smallest of the individual errors is taken as the final error estimate. Two of the three individual estimates are included in the error interval of the final estimate. From the literature value  $\nu = 0.7073(35)$ <sup>41</sup> one obtains the estimate

$$\beta_1 = 0.834(6) \quad (3.5)$$

for the surface exponent of the magnetization. For  $J_1/J = 1.5$  Eq.(3.4) does not capture the functional form of  $m_1(L)$ , because within the available range of lattice sizes the system undergoes a crossover towards the asymptotic ordinary surface critical behavior. A more detailed discussion of this crossover is postponed to Sec. 5, where the order parameter and energy density profiles are presented. If the decay of  $m_1(L)$  for  $J_1/J = 1.5$  is described by an *effective* exponent according to Eq.(3.4), one finds a value around  $0.6$  for  $L \leq 20$  and a value around  $0.9$  for  $L \geq 48$ . This indicates that only a part of the full crossover process is captured by the simulation. This leads to the conclusion that the data for  $J_1/J = 2.0$  have not yet even entered the crossover regime to ordinary surface critical behavior. It is instructive to compare these data with corresponding data for the Ising model. The surface - to - bulk coupling ratio  $J_1/J = 2.0$  already belongs to the extraordinary regime of the Ising model<sup>7</sup>, where the surface exhibits long - range order at  $T = T_c$ . The comparison is shown in Fig.2, where the data for an Ising model according to Eq.(2.1) have been obtained from a hybrid algorithm which corresponds to the one described above, except that overrelaxation moves cannot be performed in this case<sup>42</sup>. The surface magnetization decays with an effective exponent of about  $0.16$  (see Fig.2(a), solid line), whereas for the Ising model (see Fig.2(b), solid line)  $m_1(L)$  approaches the spontaneous surface magnetization  $m_{10}$  according to

$$m_1(L) = m_{10} - B_{m_1}^I L^{-\beta/\nu} \quad (3.6)$$

up to corrections to scaling, where  $\beta/\nu \simeq 0.517$ <sup>41</sup> is the scaling dimension of the order parameter in the Ising universality class and  $B_{m_1}^I$  is a nonuniversal amplitude. Fig.2 illustrates how the presence of real long - range surface order (b) can be distinguished from spurious long - range surface order (a) which only appears as

a nonasymptotic finite - size effect. However, within a typical range of numerically accessible system sizes the crossover to the asymptotic ordinary surface behavior cannot be observed for  $J_1/J \geq 2.0$  and therefore a data analysis within the framework of finite - size scaling only yields an *effective* exponent  $\beta_{1,eff} = \beta_{1,eff}(J_1/J)$ . For  $J_1/J = 2.0$  one has  $\beta_{1,eff}(2.0)/\nu \simeq 0.16$  (see Fig.2(a)) and for  $J_1/J = 3.0$  an effective exponent  $\beta_{1,eff}(3.0)/\nu \simeq 0.08$  is found (not shown). We do not quote error bars here, because the estimates for  $\beta_{1,eff}(J_1/J)$  are presumably affected by systematic errors which are larger than the statistical ones. In the interior of the system the 'bulk' magnetization  $m_b \equiv \langle m(L/2) \rangle$  obeys standard critical finite size scaling with the exponent  $\beta/\nu \simeq 0.518^{41}$  (see Eqs.(5.1) and (5.2) and Fig.10 in Sec. 5).

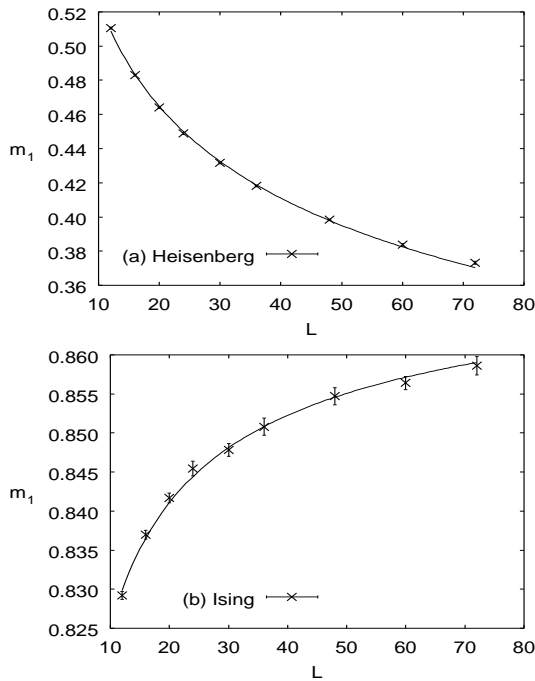


FIG. 2. Surface magnetization  $m_1(L)$  for  $J_1/J = 2.0$  at  $T = T_c$  ( $\times$ ) (a) for the Heisenberg model given by Eq.(2.1) (see also Fig.1) and (b) for a corresponding Ising model<sup>42</sup>. For the Heisenberg model (a)  $m_1(L)$  decays according to an effective power law (solid line), whereas for the Ising model (b)  $m_1(L)$  increases towards the value of the spontaneous surface magnetization according to Eq.(3.6) (solid line).

The layer susceptibility  $\chi_1$  is analyzed in the same way as the surface magnetization  $m_1(L)$ . The data are displayed in Fig.3. For  $J_1/J \leq 1$  the data can be interpreted according to

$$\chi_1(L) = B_{\chi_1} L^{\gamma_1/\nu} (1 + C_{\chi_1} L^{-\omega}), \quad (3.7)$$

which is the exact analog of Eq.(3.4). The term in parenthesis captures the leading correction to scaling,  $\gamma_1/\nu$  is the corresponding surface exponent for finite - size scaling, and  $B_{\chi_1}$  is a nonuniversal overall amplitude. With

$\omega \simeq 0.78$  as above a least square fit of Eq.(3.7) to the data shown in Fig.3 yields the estimates  $\gamma_1/\nu = 1.314(23)$ ,  $1.305(12)$ , and  $1.308(25)$  for  $J_1/J = 0.3, 0.5$ , and  $1.0$ , respectively. As before we adopt the weighted average  $\gamma_1/\nu = 1.307(12)$  as our final estimate, where the smallest of the individual errors is taken as the error estimate. From the literature value  $\nu = 0.7073(35)$  the estimate

$$\gamma_1 = 0.924(10) \quad (3.8)$$

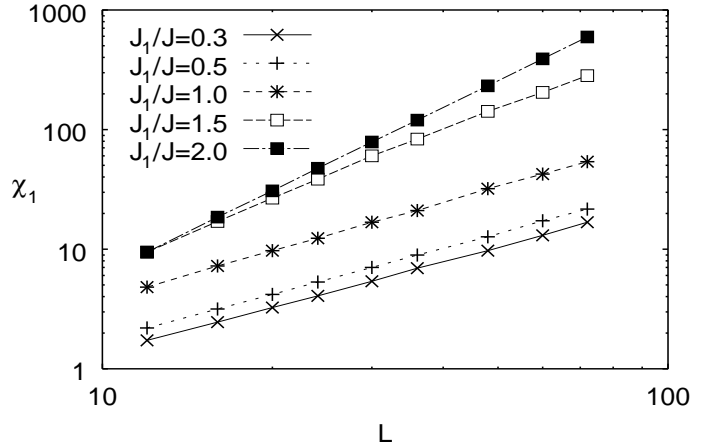


FIG. 3. Layer susceptibility  $\chi_1$  (see Eq.(3.3)) at  $T = T_c$  as function of the system size  $L$  for  $J_1/J = 0.3$  ( $\times$ , solid line),  $0.5$  ( $+$ , short dashed line),  $1.0$  ( $*$ , dashed line),  $1.5$  ( $\square$ , long dashed line), and  $2.0$  ( $\blacksquare$ , dash-dotted line). Statistical errors are smaller than the symbol sizes and the various lines are just guides to the eye. For  $J_1/J \leq 1$   $\chi_1$  displays the expected behavior for the ordinary surface universality class. For  $J_1/J = 1.5$  the system undergoes a crossover towards ordinary surface behavior, whereas for  $J_1/J = 2.0$  the behavior of  $\chi_1$  is inherently nonasymptotic within the available range of system sizes (see also Fig.1).

is found. For  $J_1/J \geq 1.5$  the data qualitatively behave as in Fig.1: For  $J_1/J = 1.5$  the system undergoes a crossover to ordinary surface behavior and for  $J_1/J = 2.0$  the asymptotic behavior is out of reach for the simulation. Nonetheless, the increase of  $\chi_1$  in the latter case can be described by an effective exponent  $\gamma_{1,eff}(J_1/J = 2.0)/\nu \simeq 2.31$ . Likewise,  $\gamma_{1,eff}(J_1/J = 3.0)/\nu \simeq 2.44$  is obtained (not shown). Error bars are not quoted for the reasons indicated above.

The exponents  $\beta_1$  and  $\gamma_1$  are not independent. From the scaling relations given by Eq.(1.3) and bulk scaling relations one can infer the simple rule  $\beta_1 + \gamma_1 = \beta + \gamma$ . From the literature<sup>41</sup> one obtains  $\beta + \gamma = 1.7557(56)$  and Eqs.(3.5) and (3.8) yield  $\beta_1 + \gamma_1 = 1.758(11)$  which verifies the above scaling law. The effective exponents  $\beta_{1,eff}(2.0)$  and  $\gamma_{1,eff}(2.0)$  for  $J_1/J = 2.0$  (see Figs.1 and 3) yield  $\beta_{1,eff}(2.0) + \gamma_{1,eff}(2.0) \simeq 1.75$  which is remarkably close to the value of  $\beta + \gamma$  quoted above. Likewise,  $\beta_{1,eff}(3.0) + \gamma_{1,eff}(3.0) \simeq 1.78$  is found for  $J_1/J = 3.0$ . From Eq.(1.3) one furthermore obtains the correlation

exponents

$$\eta_{||} = 1.358(12) \quad , \quad \eta_{\perp} = 0.697(6) \quad (3.9)$$

and the exponent

$$\gamma_{11} = -0.253(9) \quad (3.10)$$

of the surface susceptibility  $\chi_{11}$ . At  $T = T_c$  the surface susceptibility therefore behaves according to

$$\chi_{11}(L) = \chi_{110} - B_{\chi_{11}} L^{1-\eta_{||}} (1 + C_{\chi_{11}} L^{-\omega}), \quad (3.11)$$

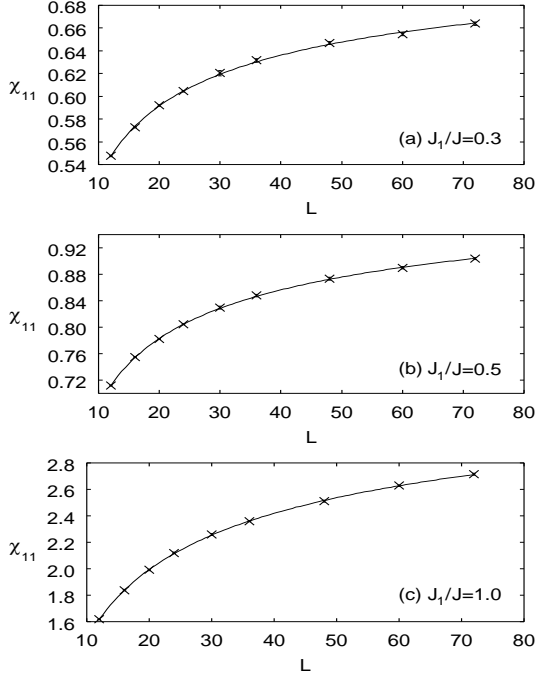


FIG. 4. Surface susceptibility  $\chi_{11}$  at  $T = T_c$  ( $\times$ ) as function of the system size  $L$  for (a)  $J_1/J = 0.3$ , (b)  $J_1/J = 0.5$ , and (c)  $J_1/J = 1.0$ . Error bars are much smaller than the symbol sizes. The solid lines display fits of Eq.(3.11) to the data (a), (b), and (c), respectively.

TABLE I. Comparison of estimates for  $\beta_1$  from experiments on Ni(100)<sup>18</sup> (average of three measurements), early Monte - Carlo work<sup>30</sup>, high temperature series<sup>16</sup>, field theory<sup>17</sup>, transfer matrix Monte - Carlo<sup>32</sup>, massive field theory<sup>12</sup> ([0/2], [2/0], [1/1] Padé approximants), and Eq.(3.5).

	Ref. <sup>18</sup>	Ref. <sup>30</sup>	Ref. <sup>16</sup>	Ref. <sup>17</sup>	Ref. <sup>32</sup>	Ref. <sup>12</sup>	Eq.(3.5)
$\beta_1$	0.81	0.75(10)	0.81(4)	0.84(1)	0.80(3)	0.862 0.889	0.834(6)

where the term in parenthesis captures the leading correction to scaling. Fits of Eq.(3.11) to the data for  $J_1/J \leq 1$  are shown in Fig.4, where  $1 - \eta_{||} = -0.358$  and  $\omega = 0.78$  are kept fixed and the amplitudes  $\chi_{110}$ ,  $B_{\chi_{11}}$

and  $C_{\chi_{11}}$  are used as fit parameters. For  $J_1/J \geq 1.5$  Eq.(3.11) does no longer describe  $\chi_{11}$  due to the strong nonasymptotic effects described above (for more details see Sec. 4). A comparison of different estimates for  $\beta_1$  from various sources is shown in Table I. The estimates are rather consistent within their mutual errors, but the best agreement is found with the field theoretic estimate given in Ref.<sup>17</sup>.

We close this section with an investigation of the finite-size behavior of the surface energy density  $e_1$ . The data for the dimensionless surface energy density  $\varepsilon_1 = e_1/(k_B T_c)$  are shown in Fig.5 for  $0.5 \leq J_1/J \leq 2.0$ . The  $L$  dependence of  $e_1$  for  $J_1/J = 0.3$  (not shown), 0.5 (a), and 1.0 (b) is qualitatively different from the  $L$  dependence for  $J_1/J = 1.5$  (c), 2.0 (d), and 3.0 (not shown). The leading  $L$  dependence of  $e_1$  is written as

$$\varepsilon_1(L) = \varepsilon_{10} + B_{e_1}^{(2)} L^{-2} + B_{e_1}^{(3)} L^{-3}, \quad (3.12)$$

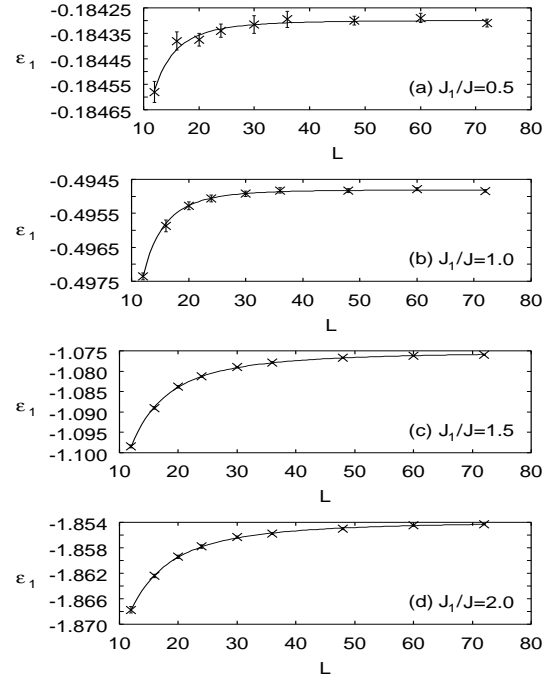


FIG. 5. Dimensionless surface energy density  $\varepsilon_1 = e_1/(k_B T_c)$  at  $T = T_c$  ( $\times$ ) as function of the system size  $L$  for (a)  $J_1/J = 0.5$ , (b)  $J_1/J = 1.0$ , (c)  $J_1/J = 1.5$ , and (d)  $J_1/J = 2.0$ . In (c) and (d) the error bars are much smaller than the symbol sizes. The solid lines display fits of Eq.(3.12) to the data (a), (b), (c), and (d), respectively.

where the amplitudes  $\varepsilon_{10}$ ,  $B_{e_1}^{(2)}$ , and  $B_{e_1}^{(3)}$  are taken as fit parameters. For  $J_1/J \leq 1$  the coefficient  $B_{e_1}^{(2)}$  turns out to be two orders of magnitude smaller than the coefficient  $B_{e_1}^{(3)}$  which suggests that  $L^{-3}$  is the leading finite - size correction in this case. According to naive finite - size scaling one expects  $x_{e_1} = (1 - \alpha_1)/\nu$  as the leading finite - size exponent for the surface energy density. In fact, due to the scaling relation  $\alpha_1 = \alpha - 1$  for the ordinary transition<sup>14,15</sup> one finds  $x_{e_1} = (2 - \alpha)/\nu = d = 3$

from hyperscaling in agreement with the simulation data in Figs.5 (a) and (b). In contrast,  $B_{e_1}^{(2)}$  and  $B_{e_1}^{(3)}$  are of roughly equal magnitude (and of opposite sign) for the case  $J_1/J \geq 1.5$  displayed in Figs.5 (c) and (d). Therefore,  $L^{-2}$  rather than  $L^{-3}$  is the leading finite - size correction here. The discrepancy between Figs.5 (a), (b) and Figs.5 (c), (d) is due to strong nonasymptotic contributions to the finite size behavior for  $J_1/J \geq 1.5$ . One possible source of the  $L^{-2}$  contribution is the scaling dimension  $x_{f_s} = (2 - \alpha_s)/\nu = (2 - \alpha - \nu)/\nu = d - 1 = 2$  of the surface free energy  $f_s$  (surface tension) which prevails in Eq.(3.12) due to the *nonscaling* dependence of the surface tension on  $J_1/J$ <sup>43</sup>. Another source of the leading  $L^{-2}$  dependence is the *regular* (noncritical) finite - size behavior of the surface tension for periodic boundary conditions<sup>43</sup>. Other finite - size corrections such as  $L^{-1}$  substantially reduce the goodness - of - fit and can therefore be ruled out as leading terms. Possible logarithmic corrections of the form  $L^{-2} \log L$ <sup>43</sup> cannot be identified unambiguously.

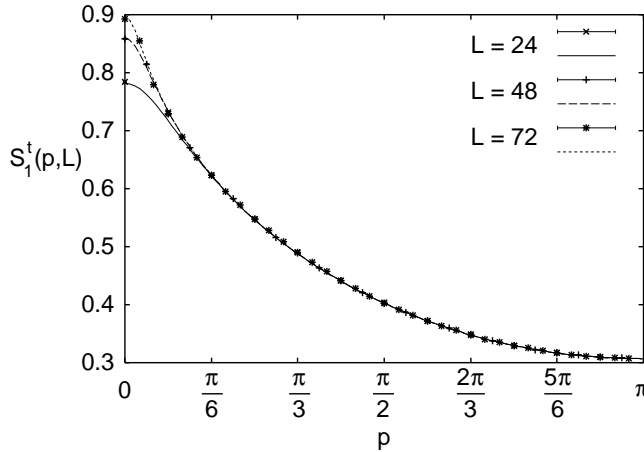


FIG. 6. Transverse component of the surface structure factor  $S_1^t(p, L)$  for  $J_1/J = 0.5$  and  $L = 24$  ( $\times$ ),  $L = 48$  ( $+$ ), and  $L = 72$  ( $*$ ) as function of the momentum transfer  $p$  in the (100) direction. Numerical evaluations of Eq.(4.2) in the limit  $c \rightarrow \infty$  for  $L = 24$ ,  $L = 48$ , and  $L = 72$  (see main text) are displayed by the solid, the long dashed and short dashed line, respectively.

#### IV. SURFACE STRUCTURE FACTOR

The surface structure factor is given by the discrete Fourier transform of the surface spin - spin correlation function

$$G_1^{\alpha\alpha}(\mathbf{x} - \mathbf{x}') = (\langle S_{x,y,1}^\alpha S_{x',y',1}^\alpha \rangle - \langle S_{x,y,1}^\alpha \rangle^2 + \langle S_{x,y,L}^\alpha S_{x',y',L}^\alpha \rangle - \langle S_{x,y,L}^\alpha \rangle^2) / 2, \quad (4.1)$$

where the Fourier transform is taken with respect to  $\mathbf{x} - \mathbf{x}'$ ,  $\mathbf{x} = (x, y)$ , and the upper index  $\alpha$  refers to the spin component. Note that off - diagonal components of  $G_1$

vanish identically. The longitudinal and transverse components of  $G_1^{\alpha\alpha}$  with respect to the total magnetization are very similar and we therefore restrict the following discussion to the transverse component only. The momentum transfer  $\mathbf{p}$  in the (100) direction, i.e., parallel to the surface, in units of the inverse lattice constant is given by  $\mathbf{p} = (p, 0, 0) = (2\pi n/L, 0, 0)$ ,  $n = 0, 1, \dots, L/2$ . Numerical data of the surface structure factor for  $J_1/J = 0.5$  in the (100) direction for three different lattice sizes are displayed in Fig.6. The data essentially collapse onto a single curve for  $p > 0$ , finite - size effects are only visible at  $p = 0$ , where the structure factor shown in Fig.6 reduces to the transverse component of the surface susceptibility  $\chi_{11}$  (see Eq.(3.11)). For  $J_1/J = 0.3$  identical properties are obtained (not shown). It turns out that lattice effects in the structure factor near the Brillouin zone boundary can be captured by the replacement  $p \rightarrow 2 \sin(p/2)$  to a remarkable accuracy<sup>44</sup>. The shape of the surface structure factor is reasonably well captured by the mean - field type expression<sup>42,44</sup>

$$S_1^\alpha(p, L) = \chi_{110}^\alpha - B_{\chi_{11}}^\alpha \frac{c^\alpha - 2 \sin(p/2)}{c^\alpha + 2 \sin(p/2)} \times \left[ \frac{2\Gamma^\alpha \sin(p/2)}{\tanh(2\Gamma^\alpha \sin(p/2)L)} \right]^{\eta_{||} - 1}, \quad (4.2)$$

where the upper index  $\alpha$  indicates the component (longitudinal  $l$  or transverse  $t$  with respect to  $\mathbf{m}_{tot}$ ) of  $S_1^\alpha(p, L)$ . The coefficients  $\chi_{110}^\alpha$  and  $B_{\chi_{11}}^\alpha$  are the coefficients of the surface susceptibility  $\chi_{11}^\alpha$  (for  $\alpha = l$  see Eq.(3.11)). The width parameter  $\Gamma^\alpha$  and the surface enhancement parameter  $c^\alpha$  are used to fit the momentum dependence of the surface structure factor and the exponent  $\eta_{||}$  is taken from Eq.(3.9). The fit is performed in two stages. First,  $\chi_{110}^\alpha$  and  $B_{\chi_{11}}^\alpha$  are determined from a least square fit of Eq.(4.2) for  $p = 0$  to the surface susceptibility. Second, the width parameter  $\Gamma^\alpha$  and, if needed (see below), the surface enhancement parameter  $c^\alpha$  are adjusted to obtain a least square fit of the momentum dependence to the data. In practice, this fit procedure has only been performed for the largest lattice size  $L = 72$ . For smaller systems the fit parameters are taken from  $L = 72$  in order to test the accuracy of the shape predicted by Eq.(4.2). The result for  $J_1/J = 0.5$  is displayed in Fig.6 for the transverse component  $S_1^t(p, L)$  of the surface structure factor. For the largest system  $L = 72$  ( $*$ ) the short dashed line shows the fit, whereas for other lattice sizes such as  $L = 24$  ( $\times$ ) and  $48$  ( $+$ ) the evaluation of Eq.(4.2) for  $L = 24$  (solid line) and  $L = 48$  (long dashed line) confirms the predicted shape to a remarkable accuracy. For  $J_1/J = 0.3$  and  $0.5$  the parameter  $c^\alpha$  is very large and therefore the surface enhancement prefactor  $(c^\alpha - 2 \sin(p/2))/(c^\alpha + 2 \sin(p/2))$  can be omitted. Noticeable deviations between the data and Eq.(4.2) for  $\alpha = t$  only occur for small  $p$  on the smaller lattices, where additional lattice corrections to Eq.(4.2) may become important. However, for any  $p > 0$  the data for all system sizes collapse onto a single curve, which can be



obtained from Eq.(4.2) by performing the limits  $c^\alpha \rightarrow \infty$  and  $L \rightarrow \infty$  at finite  $p$ .

For  $J_1/J = 1.0$  the surface enhancement parameter  $c^\alpha$  becomes important. The data are shown in Fig.7, where the surface enhancement prefactor provides an important correction to the momentum dependence of  $S_1^\alpha(p, L)$ . The fit procedure works as described above, but deviations from the assumed shape for small  $p$  also occur for  $L = 72$ . The surface structure factor is more sensitive to crossover phenomena occurring for larger values of  $J_1/J$  than the surface quantities discussed in the previous section. Corrections to scaling, which are not included in Eq.(4.2), may also account for part of the deviations between the data and the simple model for the shape function. Note that the analytic results obtained in Ref.<sup>22</sup> do not hold for the cubic geometry used here. Furthermore, nonasymptotic surface enhancement corrections, which have not been considered in Ref.<sup>22</sup>, become essential for the data analysis. For  $p > 0$  the data still collapse onto a single curve, which is given by Eq.(4.2) in the limit  $L \rightarrow \infty$  at finite  $p$  and finite  $c^\alpha \simeq 15$ .

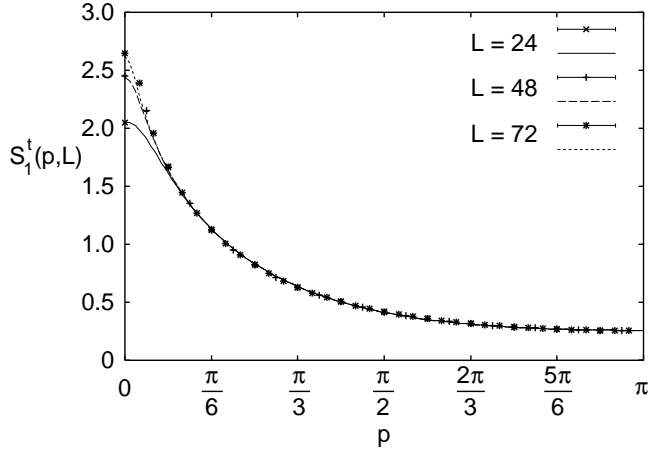


FIG. 7. Transverse component of the surface structure factor  $S_1^t(p, L)$  for  $J_1/J = 1.0$  and  $L = 24$  ( $\times$ ),  $L = 48$  ( $+$ ), and  $L = 72$  ( $*$ ) as function of the momentum transfer  $p$  in the (100) direction. Numerical evaluations of Eq.(4.2) for  $L = 24$ ,  $L = 48$ , and  $L = 72$  (see main text) are displayed by the solid, the long dashed and short dashed line, respectively. Surface enhancement corrections are essential for the data analysis.

The behavior of  $S_1^t(p, L)$  for  $J_1/J = 2.0$  is shown in Fig.8, for  $J_1/J = 3.0$  similar results have been obtained (not shown). Although scaling appears to be valid to a very high degree of accuracy, the behavior of  $S_1^t(p, L)$  is very different from Figs.6 and 7. First, the surface susceptibility *grows* according to the power law

$$\chi_{11}^\alpha(L) = B_{\chi_{11}}^\alpha L^{1-\eta_{||,eff}(J_1/J)} \quad (4.3)$$

rather than approaching a finite limit as in Eq.(3.11). From a least square fit of Eq.(4.3) to  $\chi_{11}^t$  one obtains the effective exponent  $\eta_{||,eff}(J_1/J = 2.0) \simeq -0.64$ , where deviations from the pure power law given by Eq.(4.3) are

very small. For  $J_1/J = 3.0$  one obtains  $\eta_{||,eff}(3.0) \simeq -0.82$ . We refrain from quoting error bars here, because the values for  $\eta_{||,eff}(J_1/J)$  may be affected by systematic errors due to corrections to Eq.(4.3) of unknown form. Mutual interaction between the surfaces mediated by the bulk may also cause systematic errors. With  $B_{110}^t$  and  $\eta_{||,eff}(J_1/J)$  taken from Eq.(4.3) the shape function

$$S_1^\alpha(p, L) = B_{\chi_{11}}^\alpha \frac{c^\alpha - 2 \sin(p/2)}{c^\alpha + 2 \sin(p/2)} \times \left[ \frac{2\Gamma^\alpha \sin(p/2)}{\tanh(2\Gamma^\alpha \sin(p/2)L)} \right]^{\eta_{||,eff}(J_1/J)-1}, \quad (4.4)$$

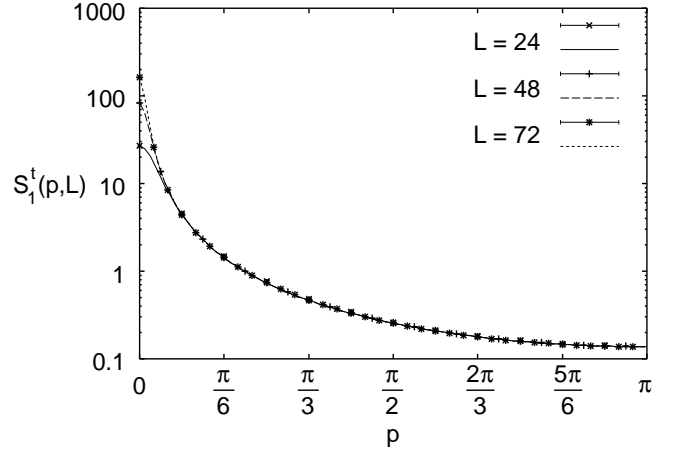


FIG. 8. Transverse component of the surface structure factor  $S_1^t(p, L)$  for  $J_1/J = 2.0$  and  $L = 24$  ( $\times$ ),  $L = 48$  ( $+$ ), and  $L = 72$  ( $*$ ) as function of the momentum transfer  $p$  in the (100) direction. Numerical evaluations of Eq.(4.4) for  $L = 24$ ,  $L = 48$ , and  $L = 72$  (see main text) are displayed by the solid, the long dashed and short dashed line, respectively. The behavior of  $S_1^t$  is inherently nonasymptotic.

is fitted to  $S_1^t$ , where the remaining two parameters  $c^\alpha$  and  $\Gamma^\alpha$  are used. As described above the fit is only performed for  $L = 72$  (short dashed line in Fig.8). For  $L = 24$  ( $\times$ ) and  $L = 48$  ( $+$ ) Eq.(4.4) ( $\alpha = t$ ) is shown for  $L = 24$  (solid line) and  $L = 48$  (long dashed line), where all fit parameters are kept fixed. The shape function given by Eq.(4.4) is remarkably accurate. However, the observed scaling is completely different from the asymptotic scaling shown in Fig.6 and, apart from surface enhancement corrections, in Fig.7. The effective exponent  $\eta_{||,eff}(J_1/J)$  is not related to the surface exponent  $\eta_{||}$  given by Eq.(3.9), because it is nonuniversal, i.e., it depends on  $J_1/J$ . From general considerations it is tempting to pose the (effective) surface scaling law  $\beta_{1,eff}(J_1/J) = \nu[d - 2 + \eta_{||,eff}(J_1/J)]/2$  (see Eq.(1.3)). The direct determination of  $\beta_{1,eff}$  from  $m_1(L)$  for  $J_1/J \geq 2.0$  is plagued with considerable uncertainties, because the decay of  $m_1(L)$  with  $L$  becomes quite slow for  $J_1/J \geq 2.0$ . Systematic errors may exceed the formal statistical error of a fit in this case and therefore the aforementioned effective scaling law cannot be con-

firmed unambiguously. Note that the crossover regime to the asymptotic scaling remains inaccessible within the range of system sizes used here. Nonetheless, the accuracy of the scaling law for  $S_1(p, L)$  for the nonasymptotic regime still lacks theoretical understanding.

For  $J_1/J = 1.5$  none of the above descriptions applies to the data and scaling appears to be violated. This is in accordance with the findings of Sec. 3, where  $m_1(L)$  and  $\chi_1(L)$  display sizable deviations from simple scaling laws. The effects of the crossover to the ordinary surface universality class are particularly pronounced in the shape function of the order parameter profile to which we turn in the following section.

## V. PROFILES

The order parameter profile  $m(z)$  (see Eq.(3.2)) provides local information about the order in the system. Furthermore,  $\langle m(z) \rangle$  is by construction very sensitive to the system size at  $T = T_c$  and should therefore be a valuable probe for scaling behavior which is easier to interpret than the structure factor. For  $J_1/J \leq 1$  all previous investigations have shown that the system essentially displays the asymptotic critical behavior of the ordinary surface universality class. The magnetization profile confirms this again, so the scaling analysis can be restricted to the case  $J_1/J = 0.5$ . The scaled magnetization profile  $M(z/L)$  is defined by

$$M(z/L) \equiv \langle m(z) \rangle / m_b, \quad (5.1)$$

where

$$m_b \equiv \langle m(L/2) \rangle = B_{m_b} L^{-\beta/\nu} (1 + C_{m_b} L^{-\omega}). \quad (5.2)$$

The factor in parenthesis captures corrections to scaling and the exponents  $\beta$ ,  $\nu$ , and  $\omega$  are taken from Ref.<sup>41</sup>. The coefficient  $C_{m_b}$  is determined by a least square fit of Eq.(5.2) to  $m_b$ . For numerical convenience  $z - 1/2$ ,  $z = 1, \dots, L$  is chosen as the position coordinate for the profile. The scaling plot for  $J_1/J = 0.5$  is shown in Fig.9, where  $z$  now refers to the *shifted* layer index. The data scale very accurately and the shape of the profile is in accordance with the expectation for the ordinary transition. The scaling function  $M(z/L)$  can be represented by the simple fit formula

$$M(\zeta) = B_M [(\zeta + \zeta_0)(1 - \zeta + \zeta_0)]^{(\beta_1 - \beta)/\nu}, \quad (5.3)$$

where  $\zeta_0 = z_0/L$  and  $z_0$  is the extrapolation length,  $\beta$  and  $\nu$  are taken from Ref.<sup>41</sup>, and  $\beta_1$  is taken from Eq.(3.5). From a least square fit of Eq.(5.3) to the data for  $L = 72$  one finds  $z_0 \simeq -0.26$  in units of the lattice constant. For  $J_1/J = 0.3$  and  $1.0$  one finds  $z_0 \simeq -0.34$  and  $z_0 \simeq 0.46$ , respectively. The choice  $0.3 \leq J_1/J \leq 1$  therefore yields quite accurate realizations of Dirichlet boundary conditions, which characterize the ordinary surface universality class.

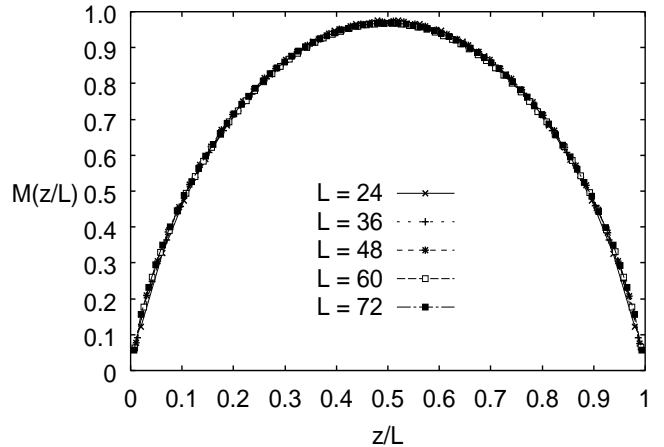


FIG. 9. Scaling function  $M(z/L)$  of the magnetization profile (see Eq.(5.1)) at  $T = T_c$  for  $J_1/J = 0.5$  and  $L = 24$  ( $\times$ , solid line), 36 ( $+$ , short dashed line), 48 ( $*$ , dashed line), 60 ( $\square$ , long dashed line), and 72 ( $\blacksquare$ , dash-dotted line). Statistical errors are much smaller than the symbol sizes and the various lines are just guides to the eye. Scaling is obtained in accordance with the ordinary surface universality class.

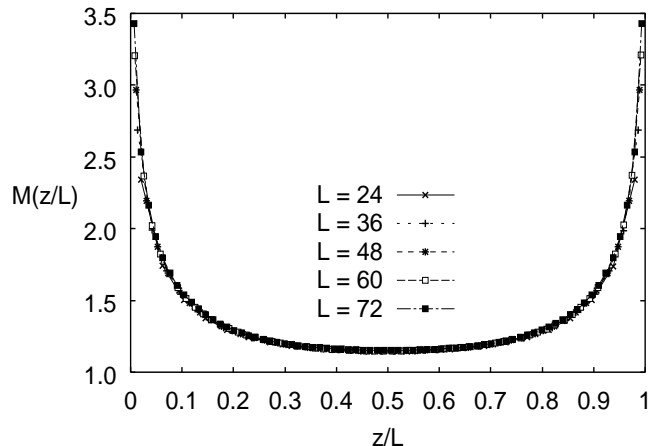


FIG. 10. Scaling function  $M(z/L)$  of the magnetization profile (see Eq.(5.1)) at  $T = T_c$  for  $J_1/J = 2.0$  and  $L = 24$  ( $\times$ , solid line), 36 ( $+$ , short dashed line), 48 ( $*$ , dashed line), 60 ( $\square$ , long dashed line), and 72 ( $\blacksquare$ , dash-dotted line). Statistical errors are much smaller than the symbol sizes and the various lines are just guides to the eye. The surface magnetization is strongly enhanced compared to the bulk magnetization (spurious long-range surface order).

For  $J_1/J = 2.0$  the application of Eqs.(5.1) and (5.2) to the data yields the result shown in Fig.10. Except at the surface layers scaling is fulfilled very accurately, however, the shape of  $m(z)$  does not show the expected fixed point form. Instead, a strong enhancement of the surface magnetization over the magnetization in the interior is obtained. A behavior like this is typical for the extraordinary transition which does *not* occur for the Heisenberg model defined by Eq.(2.1) in  $d = 3$ , i.e., the system dis-

plays *spurious* long-range surface order. If the lattice size  $L$  could be increased further one should therefore find a crossover to the ordinary behavior displayed in Fig.9 (see Fig.2). Nonetheless, the shape of the scaling function  $M(\zeta)$  is again captured by Eq.(5.3), if the exponent is used as a third fit parameter. It is tempting to write this exponent in the form  $(\beta_{1,eff}(J_1/J) - \beta)/\nu$ , however, the result for  $\beta_{1,eff}(J_1/J)$  obtained this way is not compatible with the estimate obtained from  $m_1(L)$ , which may be due to systematic errors of various kinds discussed above.

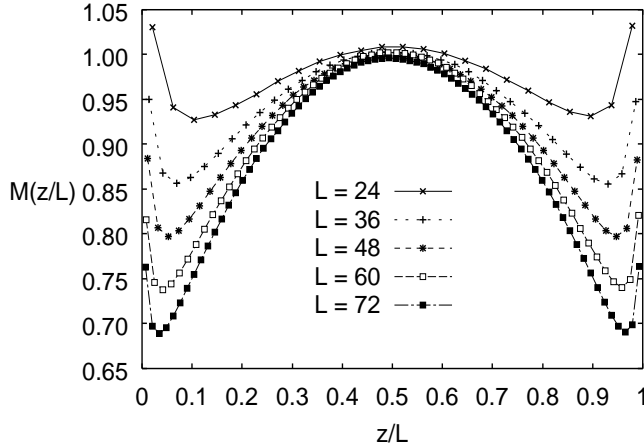


FIG. 11. Scaling plot of the magnetization profile  $M(z/L)$  (see Eq.(5.1)) at  $T = T_c$  as function of  $z/L$  for  $J_1/J = 1.5$  and  $L = 24$  ( $\times$ , solid line), 36 ( $+$ , short dashed line), 48 ( $*$ , dashed line), 60 ( $\square$ , long dashed line), and 72 ( $\blacksquare$ , dash-dotted line). Statistical errors are much smaller than the symbol sizes and the various lines are just guides to the eye. Scaling is grossly violated during the crossover from the state of spurious surface order (see Fig.10) to the ordinary surface universality class (see Fig.9) as  $L$  is increased.

The question how the system actually performs the crossover is answered in Fig.11, where  $M(z/L)$  is shown for  $J_1/J = 1.5$ . For smaller systems the surface magnetization is still enhanced over  $m_b$ , but as  $L$  is increased, the maximum of the profile at  $z = L/2$  finally exceeds  $m_1$  and the profile shape approaches the fixed point form shown in Fig.9. The influence of the surface coupling on  $\langle m(z) \rangle$  is confined to the two outermost lattice layers on either side of the cube, whereas the curvature of the remainder of the profile already has the “correct” sign for all lattice sizes shown in Fig.11. For  $L < 24$  the profile becomes flatter in the middle and the profile shape approaches the one displayed in Fig.10. Note that even at  $z = L/2$  the data fail to collapse according to Eqs.(5.1) and (5.2). Although the isotropic Heisenberg model does not display long - range surface order in the thermodynamic limit, on a *finite* lattice a strong enhancement of the surface magnetization  $m_1$  over the bulk magnetization  $m_b$  does occur for sufficiently strong surface couplings as a finite - size effect for a certain range of system sizes.

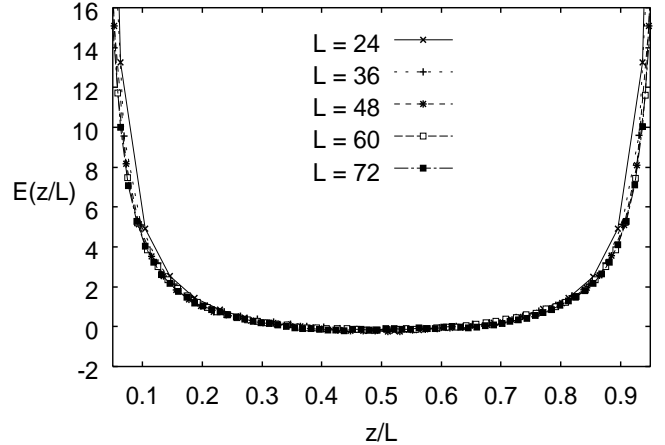


FIG. 12. Scaling function  $E(z/L)$  of the energy density profile (see Eq.(5.4)) in units of  $k_B T_c$  at  $T = T_c$  for  $J_1/J = 0.5$  and  $L = 24$  ( $\times$ , solid line), 36 ( $+$ , short dashed line), 48 ( $*$ , dashed line), 60 ( $\square$ , long dashed line), and 72 ( $\blacksquare$ , dash-dotted line). Statistical errors are smaller than the symbol sizes and the various lines are just guides to the eye. Scaling is obtained in accordance with the ordinary surface universality class.

The scaling properties of the energy density profile are a little more delicate, because a background energy density must be subtracted from the profile in order to obtain scaling. One finds the scaling form

$$E(z/L) \equiv (\langle \varepsilon(z) \rangle - \varepsilon_0)/L^{-(1-\alpha)/\nu}, \quad (5.4)$$

where  $E(\zeta)$  is the scaling function and corrections to scaling have been disregarded. For numerical convenience  $z - 1/2$ ,  $z = 1, \dots, L$  is again chosen as the position coordinate for the profile. The scaling plots for  $0.3 \leq J_1/J \leq 1.0$  are well represented by the scaling plot for  $J_1/J = 0.5$  which is shown in Fig.12. As in Figs.9 - 11  $z$  refers to the shifted layer index. The shape of the scaling function is as expected for the ordinary universality class<sup>26</sup>. For  $L > 24$  the data collapse reasonably well which confirms scaling according to Eq.(5.4), where  $(1 - \alpha)/\nu \simeq 1.586$  according to Ref.<sup>41</sup>. The shape of the scaling function  $E(\zeta)$  can be approximated by the fit formula (see also Ref.<sup>26</sup>)

$$E(\zeta) = B_E \left[ \pi / \sin \left( \pi \frac{\zeta + \zeta_0}{1 + 2\zeta_0} \right) \right]^{(1-\alpha)/\nu}, \quad (5.5)$$

where  $\zeta_0 = z_0/L$  is the scaled extrapolation length of the profile (see Eq.(5.3)). For small arguments  $\zeta = z/L$  Eq.(5.5) captures the algebraic increase of  $\langle \varepsilon(z) \rangle$  correctly and the extrapolation length  $z_0$  becomes negligibly small. However, away from the surface Eq.(5.5) captures the shape function of the energy density profile only in a qualitative sense.

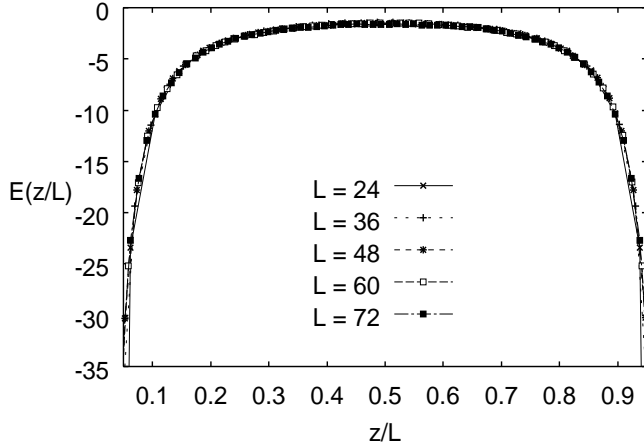


FIG. 13. Scaling function  $E(z/L)$  of the energy density profile (see Eq.(5.4)) in units of  $k_B T_c$  at  $T = T_c$  for  $J_1/J = 2.0$  and  $L = 24$  ( $\times$ , solid line), 36 ( $+$ , short dashed line), 48 ( $*$ , dashed line), 60 ( $\square$ , long dashed line), and 72 ( $\blacksquare$ , dash-dotted line). Statistical errors are smaller than the symbol sizes and the various lines are just guides to the eye. The surface energy is strongly enhanced compared to the bulk energy (see Fig10).

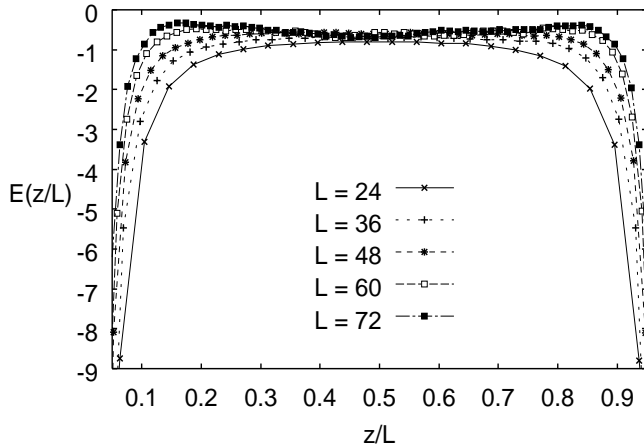


FIG. 14. Scaling plot of the energy density profile  $E(z/L)$  (see Eq.(5.4)) in units of  $k_B T_c$  at  $T = T_c$  as function of  $z/L$  for  $J_1/J = 1.5$  and  $L = 24$  ( $\times$ , solid line), 36 ( $+$ , short dashed line), 48 ( $*$ , dashed line), 60 ( $\square$ , long dashed line), and 72 ( $\blacksquare$ , dash-dotted line). Statistical errors (not shown) are slightly larger than the symbol sizes and the various lines are just guides to the eye. Scaling is grossly violated during the crossover from the state of enhanced surface energy (see Fig.13) to the ordinary surface universality class (see Fig.12) as  $L$  is increased.

For  $J_1/J = 2.0$  scaling of the data according to Eq.(5.4) works even better as shown in Fig.13. Note that the value of the reference energy density  $\varepsilon_0$  does *not* depend on  $J_1/J$ . The data for system sizes  $L \geq 24$  collapse onto a single curve, which is represented by Eq.(5.5) with a much better accuracy than for  $J_1/J \leq 1.0$ . The

extrapolation length  $z_0 \simeq -0.12$  (in units of the lattice constant) is still very small. The behavior the energy density profile displayed in Fig.13 is typical for a system at the extraordinary transition which does not exist for the Heisenberg model in  $d = 3$  with nearest neighbor interactions. According to the above discussion the shape of the energy density profile given by Fig.13 is governed by the presence of spurious long - range order in the surface. The crossover to the asymptotic shape (see Fig.12) will occur if  $L$  is increased further. For  $J_1/J = 2.0$  the crossover regime is out of reach, but for  $J_1/J = 1.5$  this crossover takes place within the range of accessible system sizes as shown in Fig.14. As in Fig.11 scaling is violated. The curvature of the profile near  $z = L/2$  changes sign between  $L = 36$  and  $L = 60$  and for  $L \geq 60$  the profile approaches its asymptotic shape. The nonasymptotic surface effects are more pronounced here than for the magnetization profile and penetrate deeper into the system, but the magnitude of the surface induced enhancement of the energy density at the surface decays quickly with increasing  $L$ . The same crossover behavior can be observed for the critical Ising model slightly below the  $SB$  multicritical point for, e.g.,  $J_1/J = 1.45^{42}$ .

## VI. SUMMARY AND OUTLOOK

In the absence of symmetry breaking fields the asymptotic critical scaling behavior of surfaces of a critical  $d = 3$  dimensional Heisenberg magnet with short - range interactions is always governed by the ordinary surface universality class. For finite systems, however, a crucial interplay between the available system size and the value of the surface - to - bulk coupling ratio  $J_1/J$  determines whether or not the asymptotic surface scaling behavior can actually be observed. Within the range of system sizes  $12 \leq L \leq 72$  for the  $L \times L \times L$  geometry used here critical behavior in the ordinary surface universality class can be observed for  $J_1/J \leq 1.0$ . The scaling exponents found numerically in this case are consistent with rigorous scaling laws and estimates for these exponents found previously by various analytical and numerical methods. The shape of the surface structure factor  $S_1(p, L)$  is captured by very simple mean - field like expressions, in which two amplitudes are fixed by a fit to the surface susceptibility for  $p = 0$ . A width parameter and, if needed, a surface enhancement parameter then determine the shape of the momentum dependence. It turns out, that finite - size and lattice effects are very accurately described by the pseudo scaling argument  $2 \sin(p/2)L$  which replaces the true scaling argument  $pL$ . These properties of  $S_1(p, L)$  are essential for the data interpretation of the *dynamic* surface structure factor which is the key quantity for the interpretation of neutron scattering data on magnetic surfaces and will therefore be the main focus of ensuing work. The order parameter and energy density profiles are less relevant

for experiments, but they are easier to interpret and yield valuable insight into the scaling behavior of the system. Either profile is found to scale in accordance with the ordinary surface universality class.

For  $J_1/J \geq 2.0$  scaling is still found for all quantities under investigation, however, the scaling exponents are replaced by effective ones and their values depend on  $J_1/J$ . The scaling relations cannot be verified unambiguously, because some of the numerical estimates for the effective exponents are presumably affected by systematic errors of unknown magnitude. Such errors may ensue due to unknown corrections to the effective scaling laws or due to an effective interaction between the two surfaces mediated by the bulk system in between. Nonetheless, the effective scaling properties of the surface structure factor  $S_1(p, L)$  provide valuable information for the analysis of its dynamic counterpart. The striking scaling properties found here still await theoretical explanation.

Coupling ratios  $J_1/J \geq 2.0$  are too large to access the crossover regime from the state of enhanced surface magnetization (spurious long - range surface order) to the asymptotic (ordinary) surface scaling. For  $J_1/J = 1.5$ , however, this crossover becomes the dominating feature in the finite - size behavior of all quantities under investigation, at least within the range of system sizes used here. The value  $J_1/J = 1.5$  only marks the location of the crossover regime for the system sizes at hand rather than a sharp transition in the surface behavior of the Heisenberg model. In the crossover regime scaling is violated and further theoretical insight is needed for a purposeful data analysis. Scaling of bulk quantities is also affected by particularly large correction terms. The crossover process itself is best visualized in the shape crossover of the magnetization and the energy density profiles, which occurs as  $L$  is increased for  $J_1/J = 1.5$  and  $T = T_c$ .

## ACKNOWLEDGMENTS

The author gratefully acknowledges financial support of the major part of this work through the Heisenberg program of the Deutsche Forschungsgemeinschaft under grant # Kr 1322/2-1.

---

<sup>1</sup> K. Binder, in *Phase Transitions and Critical Phenomena*, edited by C. Domb and J. L. Lebowitz (Academic, London, 1983), Vol. 8, p. 2.

<sup>2</sup> H. W. Diehl, in *Phase Transitions and Critical Phenomena*, edited by C. Domb and J. L. Lebowitz (Academic, London, 1986), Vol. 10, p. 76.

<sup>3</sup> H. W. Diehl, Int. J. Mod. Phys. B **11**, 3503 (1997).

<sup>4</sup> M. E. Fisher and P. J. Upton, Phys. Rev. Lett. **65**, 3405 (1990).

- <sup>5</sup> T. W. Burkhardt and H. W. Diehl, Phys. Rev. B **50**, 3894 (1994).
- <sup>6</sup> N. D. Mermin and H. Wagner, Phys. Rev. Lett. **17**, 1133 (1966).
- <sup>7</sup> C. Ruge and F. Wagner, Phys. Rev. B **52**, 4209 (1995).
- <sup>8</sup> P. Peczak and D. P. Landau, Phys. Rev. B **43**, 1048 (1991).
- <sup>9</sup> M. Yu. Nalimov, Theor. and Math. Phys. **102**, 163 (1995).
- <sup>10</sup> X. S. Chen, V. Dohm, and N. Schultka, Phys. Rev. Lett. **77**, 3641 (1996).
- <sup>11</sup> H. W. Diehl and S. Dietrich, Z. Phys. B **42**, 65 (1981).
- <sup>12</sup> H. W. Diehl and M. Shpot, Phys. Rev. Lett. **73**, 3431 (1994); Nucl. Phys. **B528**, 595 (1998).
- <sup>13</sup> S. Dietrich and H. W. Diehl, Z. Phys. B **43**, 315 (1981).
- <sup>14</sup> H. W. Diehl, S. Dietrich, and E. Eisenriegler, Phys. Rev. B **27**, 2937 (1983).
- <sup>15</sup> T. W. Burkhardt and J. Cardy, J. Phys. A **20**, L233 (1987).
- <sup>16</sup> K. Ohno, Y. Okabe, and A. Morita, Prog. Theor. Phys. **71**, 714 (1984).
- <sup>17</sup> H. W. Diehl and A. Nüsser, Phys. Rev. Lett. **56**, 2834 (1986).
- <sup>18</sup> S. Alvarado, M. Campagna, and H. Hopster, Phys. Rev. Lett. **48**, 51 (1982); S. Alvarado, M. Campagna, F. Ciccaci, and H. Hopster, J. Appl. Phys. **53**, 7920 (1982).
- <sup>19</sup> H. Dosch, *Critical Phenomena at Surfaces and Interfaces: Evanescent X - Ray and Neutron Scattering*, Springer Tracts in Modern Physics Vol. 126 (Springer, Heidelberg, 1992).
- <sup>20</sup> A. M. Nemirovsky and Karl F. Freed, Nucl. Phys. **B270**, 423 (1986).
- <sup>21</sup> A. M. Nemirovsky, Zhen - Gang Wang, and Karl F. Freed, Phys. Rev. B **36**, 3755 (1987).
- <sup>22</sup> R. Klimpel and S. Dietrich, Phys. Rev. B **60**, 16977 (1999).
- <sup>23</sup> T. W. Burkhardt and T. Xue, Phys. Rev. Lett. **66**, 895 (1991).
- <sup>24</sup> T. W. Burkhardt and E. Eisenriegler, Nucl. Phys. **B424**, 487 (1994).
- <sup>25</sup> E. Eisenriegler, M. Krech, and S. Dietrich, Phys. Rev. Lett. **70**, 619 (1993), **70**, 2051 (1993); Phys. Rev. B **53**, 14377 (1996).
- <sup>26</sup> M. Krech, E. Eisenriegler, and S. Dietrich, Phys. Rev. E **52**, 1345 (1995).
- <sup>27</sup> U. Ritschel and P. Czerner, Phys. Rev. Lett. **77**, 3645 (1996).
- <sup>28</sup> A. Drewitz, R. Leidl, T. W. Burkhardt, and H. W. Diehl, Phys. Rev. Lett. **78**, 1090 (1997); R. Leidl and H. W. Diehl, Phys. Rev. B **57**, 1908 (1998).
- <sup>29</sup> H. Müller - Krumbhaar and K. Binder, Z. Phys. **254**, 269 (1972); K. Binder and H. Müller - Krumbhaar, Phys. Rev. B **7**, 3297 (1973).
- <sup>30</sup> K. Binder and P. C. Hohenberg, Phys. Rev. B **9**, 2194 (1974).
- <sup>31</sup> H. Müller - Krumbhaar, J. Phys. C **9**, 345 (1976).
- <sup>32</sup> M. P. Nightingale and H. W. J. Blöte, Phys. Rev. Lett. **60**, 1562 (1988).
- <sup>33</sup> D. P. Landau and K. Binder, Phys. Rev. B **41**, 4633 (1990); K. Binder, D. P. Landau, and A. M. Ferrenberg, Phys. Rev. Lett. **74**, 298 (1995).
- <sup>34</sup> D. P. Landau, R. Paudey, and K. Binder, Phys. Rev. B **39**, 12302 (1989).
- <sup>35</sup> M. Pleimling and W. Selke, Eur. Phys. J. B **1**, 385 (1998).

- <sup>36</sup> H. W. Diehl, Eur. Phys. J. B **1**, 404 (1998).
- <sup>37</sup> K. Chen, A. M. Ferrenberg, and D. P. Landau, Phys. Rev. B **48**, 3249 (1993).
- <sup>38</sup> U. Wolff, Phys. Rev. Lett. **62**, 361 (1989).
- <sup>39</sup> A. M. Ferrenberg, D. P. Landau, and Y. J. Wong, Phys. Rev. Lett. **69**, 3382 (1993); L. N. Shchur and H. W. J. Blöte, Phys. Rev. E **55**, R4905 (1997).
- <sup>40</sup> A. M. Ferrenberg and D. P. Landau, unpublished.
- <sup>41</sup> R. Guida and J. Zinn - Justin, J. Phys. A. **31**, 8103 (1998).
- <sup>42</sup> M. Krech, unpublished.
- <sup>43</sup> V. Privman, *Finite Size Scaling and Numerical Simulation of Statistical Systems*, World Scientific, Singapore (1990).
- <sup>44</sup> C. Ruge, P. Zhu, and F. Wagner, Physica A **209**, 431 (1994).